Supplementary Information

Quantum transport properties of single-crystalline $Ag_2Se_{0.5}Te_{0.5}$ nanowire as a new topological material

Minjin Kim,[a] Jihwan Kim,[b] In-Ho Lee,[b] Woo Hyun Han,[c] Yun Chang Park,[d] Woo Youn Kim,[*a] Bongsoo Kim[*a] and Junho Suh[*b]

[a]*Department of Chemistry, KAIST, Daejeon 34141, Korea.*

[b]*Korea Research Institute of Standards and Science, Daejeon 34113, Korea.*

[c]*Department of Physics, KAIST, Daejeon 34141, Korea.*

[d]*Department of Measurement and Analysis, National Nanofab Center, Daejeon 34141, Korea.*

*Corresponding authors: wooyoun@kaist.ac.kr; comnsi@gmail.com; junho.suh@kriss.re.kr

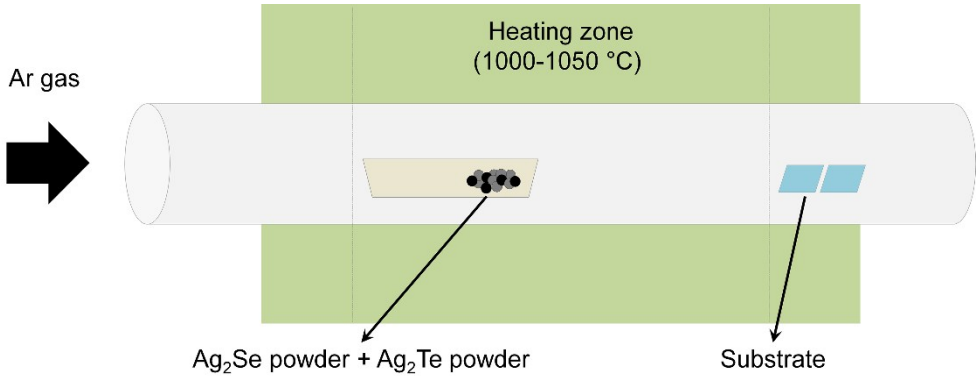

Figure S1. Schematic of the experimental setup for the synthesis of $Ag_2Se_xTe_{1-x}$ NWs, nanoribbons, and nanoplates.

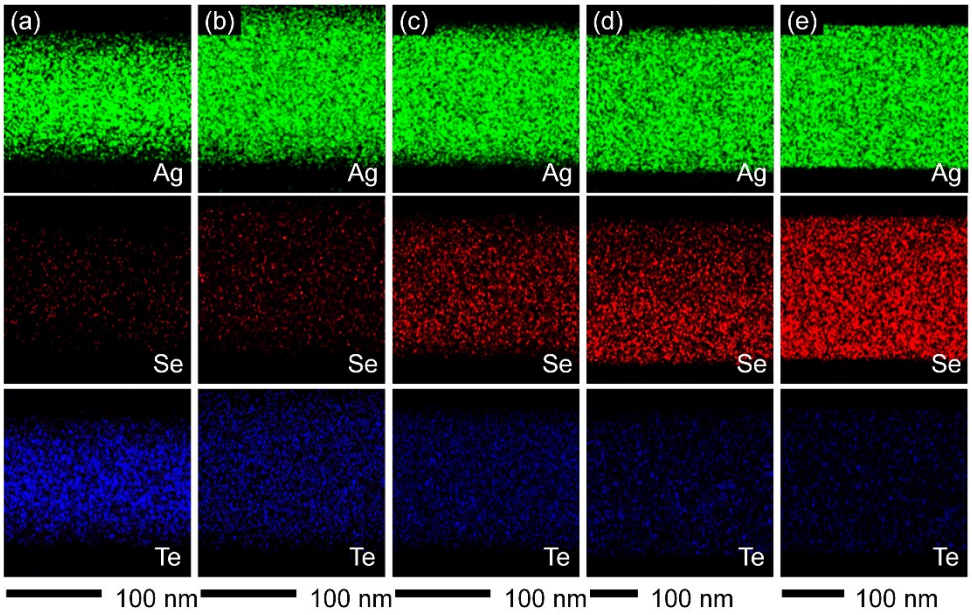

Figure S2. Representative EDS elemental mapping images of five $Ag_2Se_xTe_{1-x}$ NWs with different chemical compositions: x = (a) 0.18, (b) 0.26, (c) 0.52, (d) 0.78, and (e) 0.88. The corresponding mole fractions of the Ag_2Se powder in the precursor, $X_{Precursor}$, are (a) 0.17, (b) 0.25, (c) 0.50, (d) 0.75, and (e) 0.83, respectively.

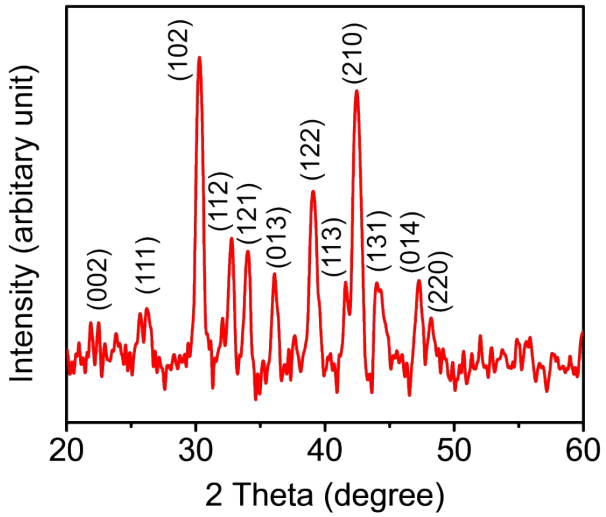

Figure S3. X-ray diffraction (XRD) pattern of synthesized $Ag_2Se_{0.5}Te_{0.5}$ nanostructures. The diffraction peaks are identified based on the orthorhombic crystal structure with lattice parameters of a = 4.43 Å, b = 7.23 Å, and c = 7.97 Å.

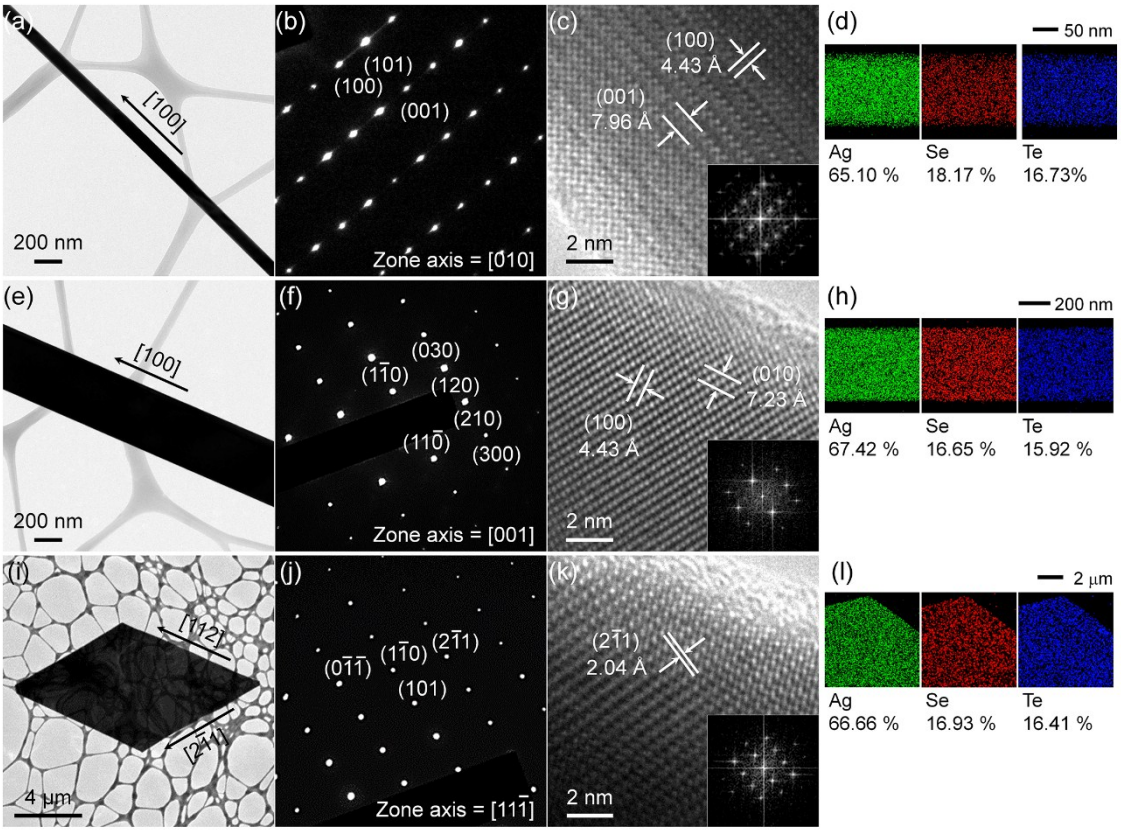

Figure S4. TEM and EDS analyses of $Ag_2Se_{0.5}Te_{0.5}$ (a–d) NW, (e–h) nanoribbon, and (i–l) nanoplate. (a), (e), and (i) are low-resolution TEM images of $Ag_2Se_{0.5}Te_{0.5}$ NW, nanoribbon, and nanoplate, respectively. (b), (f), and (j) are the corresponding SAED patterns along the various zone axis. The high-resolution TEM images ((c), (g), and (k)) and FFT patterns (insets in (c), (g), and (k)) verify the single-crystallinity without defects and orthorhombic structure with lattice parameters of a = 4.43 Å, b = 7.23 Å, and c = 7.97 Å. The growth direction of NWs and nanoribbons is [100]. EDS elemental mapping images (d), (h), and (l) with atomic percentages indicate that Ag, Se, and Te atoms are uniformly distributed in the nanostructures with an element composition of Ag:Se:Te = 2:0.5:0.5.

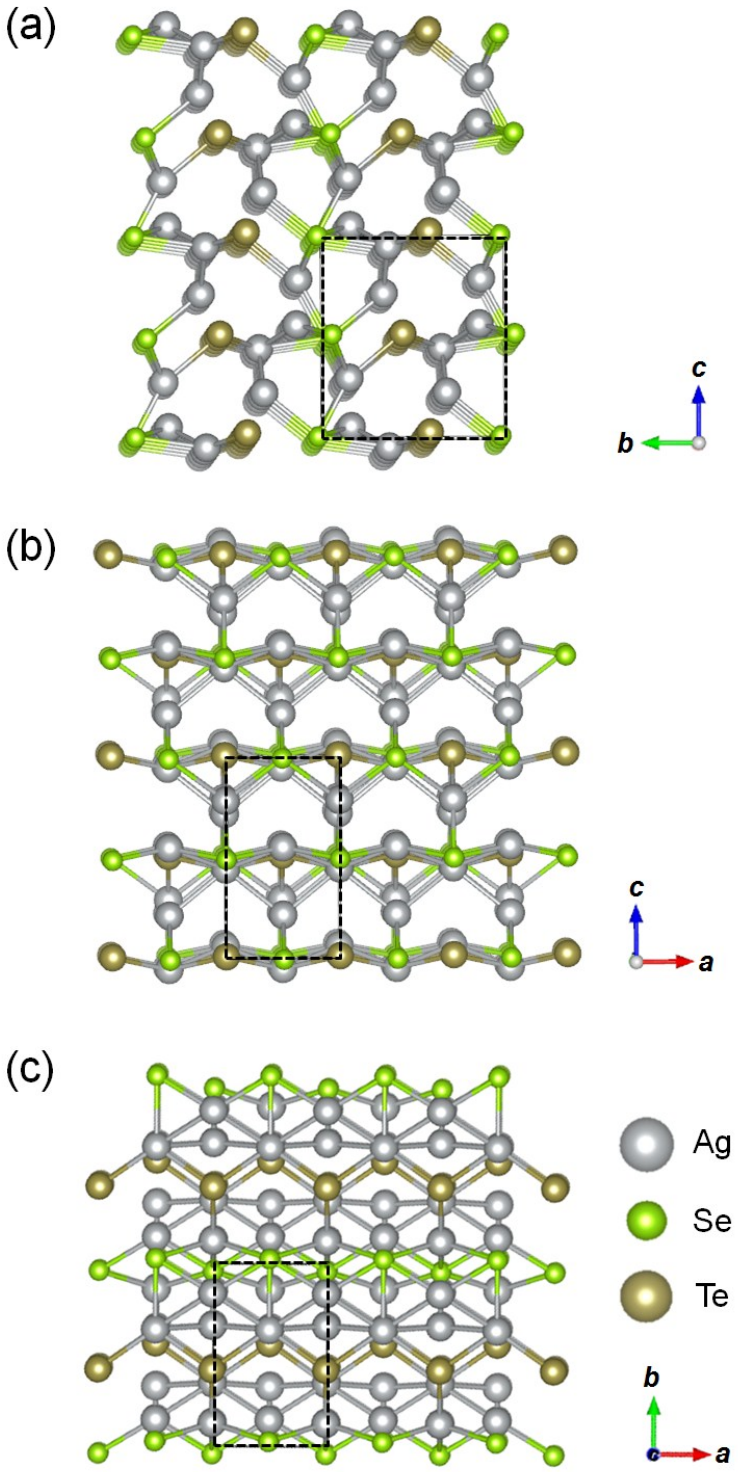

Figure S5. Schematics of expected $Ag_2Se_{0.5}Te_{0.5}$ orthorhombic crystal structure (*Pmn2*$_1$, space group number 31). The schematics are along (a) *a*, (b) *b*, and (c) *c* axis. The dashed lines indicate the primitive unit cell.

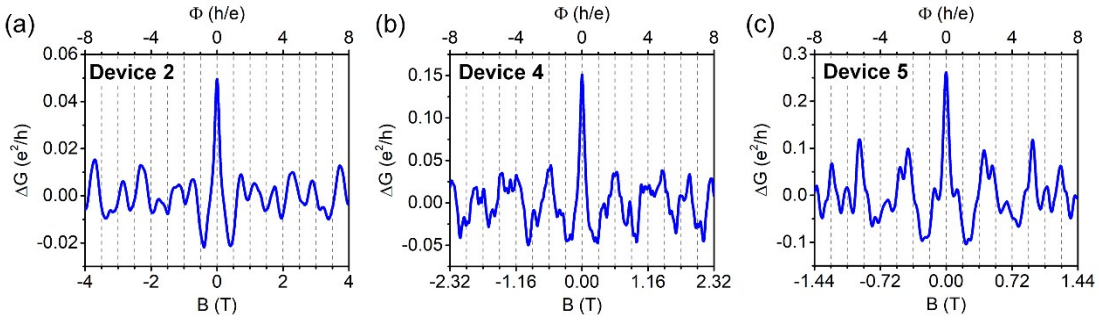

Figure S6. Aharonov–Bohm (AB) oscillations in the $Ag_2Se_{0.5}Te_{0.5}$ NW at 2 K. (a) Magneto-conductance change ΔG curve from device 2 with NW dimensions of thickness = 105 nm and width = 85 nm. The oscillation period is ΔB = 0.50 T, which is close to the estimated $\Delta B = \Phi_0/S$ = 0.46 T with cross-sectional area $S = 0.89\times10^{-14}$ m^2. (b) Magneto-conductance change ΔG curve from device 4 with NW dimensions of thickness = 118 nm and width = 113 nm. The oscillation period is ΔB = 0.29 T, which is close to the estimated $\Delta B = \Phi_0/S$ = 0.31 T with cross-sectional area $S = 1.33\times10^{-14}$ m^2. (c) Magneto-conductance change ΔG curve from device 5 with NW dimensions of thickness = 140 nm and width = 160 nm. The oscillation period is ΔB = 0.18 T, which agrees well with the estimated $\Delta B = \Phi_0/S$ = 0.18 T with cross-sectional area $S = 2.24\times10^{-14}$ m^2.

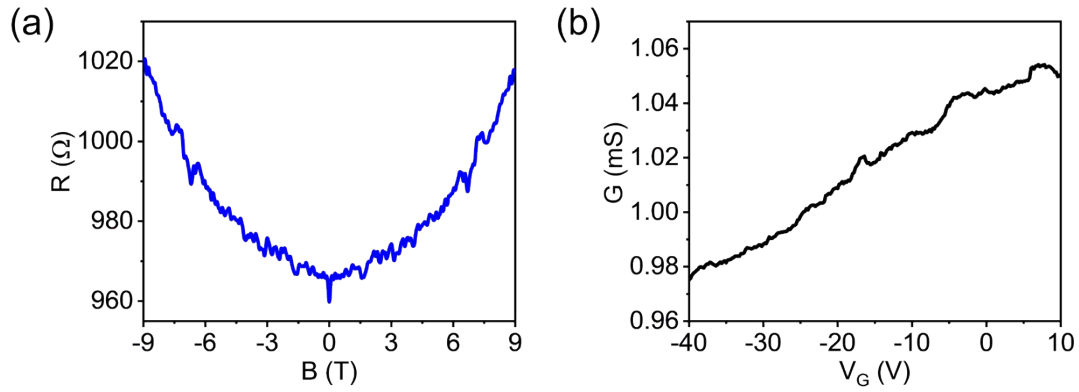

Figure S7. (a) Longitudinal magneto-resistances R versus magnetic field B curve and (b) Gate V_G dependent conductance G (= $1/R$) curve from device 3. The FET mobility μ is obtained by $\mu = (dG/dV_G)(L^2/C)$, where dG/dV_G is the linear slope of gate dependent G curve, L is the channel length, and C is the capacitance between the gate and nanowire. With $dG/dV_G = 1.7\times10^{-6}$ S/V, L = 1.3 μm, and $C = 2.1\times10^{-17}$ F, mobility μ is 1330 $cm^2s^{-1}V^{-1}$. The carrier concentration n is obtained by $n = \sigma_{xx}/e\mu$, where e is elementary charge and σ_{xx} is assumed as $1/\rho_{xx} = L/R_{xx}A$. With L = 1.3 μm, $A = 2.25\times10^{-14}$ m^2, longitudinal magneto-resistances $R = R_{xx}$ = 990 Ω (B = 6 T) and the mobility μ, n is 2.66×10^{24} m^{-3}. Then, the transverse magneto-resistances R_{xy} value can be obtained by $R_{xy} = B/nte$. Using the obtained carrier concentration n, nanowire thickness t = 155 nm, and magnetic field B = 6 T, R_{xy} is estimated to be as 88 Ω, which is much less than R_{xx} and makes it reasonable to obtain the Landau fan diagrams from R_{xx}.

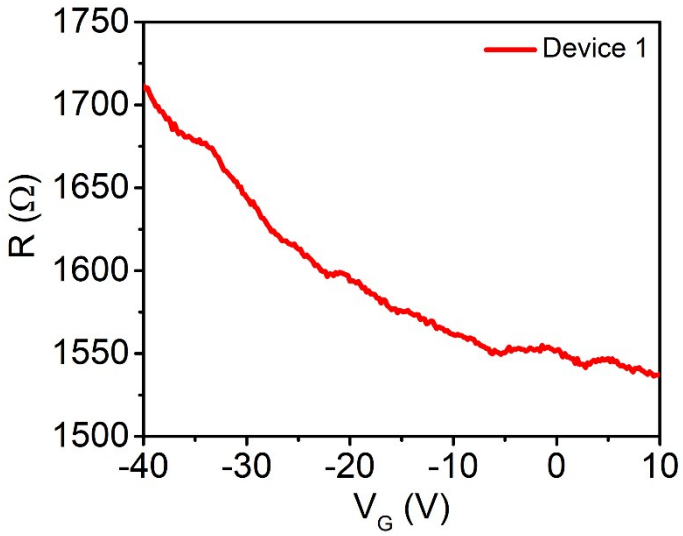

Figure S8. Back-gate dependence of $Ag_2Se_{0.5}Te_{0.5}$ NW resistance. The NW shows an *n*-type semiconductor response, and the Fermi level is located away from the Dirac point.

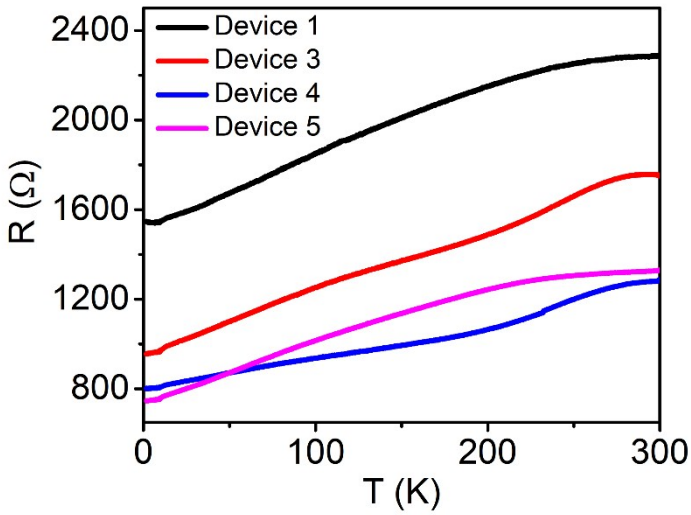

Figure S9. Temperature dependence of $Ag_2Se_{0.5}Te_{0.5}$ NW resistance, showing a typical temperature response of a metal.

Table S1. Atomic coordinates of Ag, Se, and Te in $Ag_2Se_{0.5}Te_{0.5}$ structure (space group $Pmn2_1$) used for the band structure calculation.

Atom	***x***	***y***	***z***
Ag(1)	0.00000	0.35192	0.44309
Ag(2)	0.50000	0.86469	0.28640
Ag(3)	0.50000	0.33163	0.21459
Ag(4)	1.00000	0.84832	0.05283
Ag(5)	0.50000	0.15168	0.55283
Ag(6)	0.00000	0.66837	0.71459
Ag(7)	0.00000	0.13531	0.78640
Ag(8)	0.50000	0.64808	0.94309
Se(1)	0.50000	0.03614	0.99557
Se(2)	1.00000	0.96386	0.49557
Te(1)	0.50000	0.57054	0.50753
Te(2)	1.00000	0.42946	0.00753

Table S2. Parameters of the topological surface states obtained from SdH oscillation at 2 K using LK analysis

B_F [T]	μ [$cm^2s^{-1}V^{-1}$]	γ	n_{2D} [$\times 10^{12}$ cm^{-2}]	k_F [nm^{-1}]	l_e [nm]
44.5 ± 0.3	2300 ± 230	0.40 ± 0.04	1.08 ± 0.01	0.368 ± 0.001	55.6 ± 6.3

Table S3. Parameters obtained from the temperature dependence of SdH oscillation using LK analysis

m^* [m_e]	V_F [$\times 10^5$ ms^{-1}]	E_F [meV]	τ [$\times 10^{-14}$ s]	T_D [K]	l_e [nm]	μ [cm^{2}s^{-1}V^{-1}]
0.096 ± 0.011	4.42 ± 0.50	53.5 ± 6.1	11.7 ± 1.3	10.4 ± 1.2	51.5 ± 8.3	2130 ± 340